Active saltwater intrusion of shrinking Bakhtegan -Thask Lakes in South Iran threatens the freshwater resources of coastal aquifers

Maryam Vahidipour [a], Ezzat Raeisi [a,*], Sjoerd E.A.T.M. van der Zee [b,c]

[a] Department of Geology, Faculty of Sciences, Shiraz University, 7146713565, Shiraz, Iran
[b] Soil Physics and Land Management Group, Wageningen University, P.O. Box 47, 6700 AA, the Netherlands
[c] School of Chemistry, Monash University, Melbourne, VIC, 3800, Australia

A B S T R A C T

Study region: Eight Coastal aquifers (CA) of Bakhtegan and Tashk lakes (BTL) and salt marsh, southern Iran

Study focus: BTL, Wetlands of International Importance, have been shrinking due to reduction in surface discharge, groundwater overexploitation, and drought. We show that this resulted in an increase of BTL total dissolved solids (TDS) from 45400 to 256000 mg/l. To characterize the hydrogeological behavior of the coastal aquifers after shrinkage, major ions, TDS and water level were measured along a transect from inside the BL to one of the aquifers. The spatial distribution of electrical conductivity (EC), discharge and iso-potential maps was determined. A support vector regression technique was used to forecast EC and water level in CA for the next decade.

New hydrological insights for the region: Five zones based on EC changes and hydraulic gradient are recognized, namely: brine, highly saline, brackish, transition, and freshwater. The groundwater flow direction is from both the BTL and Fresh Water Zone, converging towards the intermediately positioned Transition Zone. Saltwater intrusion is active based on the hydraulic gradient towards the land and the gradient of water density. A schematic flow model of CA was proposed based on active SWI, groundwater flow direction, and chemical signature. Forecasting reveals a significant further deterioration of water quality and drop in groundwater levels, which emphasizes the need for systematic and sustainable water management.

1. Introduction

Coastal aquifers are the primary source of freshwater for up to one billion people worldwide (Small and Nicholls, 2003). Sea or saltwater intrusion (SWI) is the landward movement of sea or saltwater into coastal aquifers. The driving force is usually the density gradient between fresh and saltwater and the hydraulic gradient of the water level between sea and the coastal aquifer (Bear, 1979). SWI has been classified into passive, where the hydraulic head (freshwater) decreases in the seaward direction, passive-active, where the gradient decreases in both landward and seaward directions from a groundwater mound, and active SWI, the hydraulic gradient of saline water slopes towards the land, due to forces by density differences, causing more aggressive salinization and fresh groundwater flow also act in the same direction, (Werner, 2017). Active SWI occurs where the salt-fresh interface is unstable, this occurs when all the heads within the coastal aquifer are lower than the density corrected head at the base of aquifers. Then, the hydraulic gradient

changes landwards and the sea or saltwater intrude into the coastal aquifer, replacing freshwater (Morgan and Werner 2015).

Many studies focused on passive SWI because it is common in most coastal aquifers (i.e., Telahigue et al., 2020; Ju et al., 2020). In passive SWI, the position and characteristics of the mixing zone are often well known, and its upper part coincides with the coastline intersecting the aquifer (Bear, 1972; Glover, 1959; Werner et al., 2013).

Active SWI leads to more aggressive salinization and is observed in many areas (i.e., Yakirevich et al., 1998; Fetter, 2001; Werner and Gallagher, 2006; Morgan and Werner, 2015), even though, it has received considerably less attention than passive SWI (Badaruddin et al., 2017).

Vázquez-Suñé et al. (2006) studied the Llobregat Delta (Spain), where groundwater levels fell to more than 25 m below sea level and created active SWI conditions, which led to rapid and extensive salinization of the coastal aquifers.

Badaruddin et al. (2015) applied physical experiments and numerical modeling to study active SWI in various nontidal, unconfined coastal aquifer. Laboratory experiments and numerical simulations for non-tidal unconfined coastal aquifers show that freshwater hydraulic gradients slope toward the land because freshwater ceased to discharge into the sea in the absence of significant recharge. Morgan and Werner (2015) used a steady-state analytic approach to quantify seawater extent in many of Australia's unconfined and confined coastal aquifers. They indicated that active seawater intrusion conditions occur in many of Australia's confined coastal aquifers.

Badaruddin et al. (2017) used numerical modeling of various idealized unconfined coastal aquifer settings to determine relationships between interface characteristics such as slope, mixing zone thickness and movement rate and mixing zone thickness as a function of freshwater-seawater density contrast, dispersity, hydraulic conductivity, porosity and aquifer thickness. The interface between freshwater and saline water migrates faster with higher hydraulic conductivity, lower effective porosity (n), steeper hydraulic gradient and greater density difference between freshwater and seawater.

Stoeckl et al. (2019) used laboratory scale physical experiments and numerical modeling to study post-pumping seawater intrusion (PP-SWI). As a result of pumping, water entered the model from both sides, from the coastal boundary as seawater and from the inland boundary as freshwater, to fill up the cone of depression. When pumping was discontinued, the cone of depression moved inland, which caused water to flow from the coast and inland in order to fill the depression cone. As a result, the saltwater wedge moved landward after the pumping cessation until recovering the depression cone. Walther and Leonard (2020) extended the work of Stoeckl et al. (2019) by evaluating the sensitivity of the PP-SWI to pump rate and distance from the coast. The results indicate that PP-SWI does not occur below a minimum pump rate and there is no relation with pump distance from the coast.

Efforts towards recognition of active SWI phenomena are limited and mainly rely on numerical modeling and laboratory experiments. Research on hydrochemistry and hydrogeological characteristics of coastal aquifers based on field data under active SWI are limited especially under drought conditions, shrinkage of salt lakes and overexploitation.

Iran, being in the zone with semi-arid and arid conditions, is confronted with salinity hazards. Iran has 250 wetlands with an area of 2.5 million hectares, and 24 wetlands with a total area of 1.48 million ha registered in Ramsar Convention's List of International Wetlands. Among these, 6 wetlands including Bakhtegan - Tashk, Kamjan, Shadegan, Anzali, Shurgol, Hamun-e-Helmand, and Hamun-e-Puzak & Hamun-e-Saberi are in the Montreux Records. The Montreux Record is a record of the Ramsar sites where changes in ecological characters have occurred, or are likely to occur.

The hypersaline Bakhtegan and Tashk Lakes (BTL) (located in the southern part of Iran) are the second-largest inland water body in Iran. The BTL was registered as a national park in 1995. A total of 86 mammal, 218 bird, 30 reptile and 23 fish species have been identified in the BTL (Fotooli, 2002). The BTL shrunk significantly since 2007 due to overexploitation of groundwater by production wells, drought, and recently the construction of two dams: Mollasadra and Sivand. The drying of a vast area of the Bakhtegan wetland in Iran resulted in the major mortality of flamingo chicks in 2007 (Ganjali and Ildoromi, 2012).

However, the impact of the shrinking of BTL causes additional concerns including: (1) transport of salt and dust from the exposed lake bed to adjacent cities and villages, (2) reduction of the evaporation and humidity, (3) decrease of birds migration, (4) decreasing attractiveness for tourists, (5) increasing contaminant concentrations of water and lake sediment, and (6) enhancement of saltwater intrusion into the adjacent aquifers. The average Total Dissolved Solids (TDS) of the BTL was 45400 mg/l before shrinkage (2007) and it increased to average 256000 mg/l after 2007. The BTL is surrounded by six aquifers and a salt marsh to the west and the salt marsh is also in direct contact with two aquifers. These 8 aquifers are named coastal aquifers (CA). The water of the coastal aquifers has a TDS signature with concentrations up to about 13000 mg/l (Fars Regional Water Authority (FRWA, 2009) near the lakes and it changes to freshwater at a higher elevation. The depth to water table is more than 5 m in dry and wet seasons. The salinity sources in the vicinity of coastal aquifers are the BTL and salt marsh. The water of BTL and salt marsh has a large enough salinity to cause saltwater intrusion into the coastal aquifers.

No systematic investigation has yet been done concerning saltwater intrusion of the BTL coastal aquifers, which might invoke unproperly focused counter-measures. Some evidence has been provided that groundwater close to the BTL and salt marsh, both the electrical conductivity (EC) and total dissolved solids in water (TDS), increase significantly and exceed the concentrations that are compatible with agriculture (Bastani and Rakhshandehroo, 2010; Afrasiabi and Sedghi Asl, 2015). Our aim is to provide evidence of the type of Salt Water Intrusion (SWI) (passive or active) in the coastal aquifers of BTL. Both the geometry and the transition of properties of the mixing zone in the coastal aquifers are characterized geohydrologically and hydrochemically. Based on this characterization, we infer a general spatiotemporal understanding and conceptual model concerning SWI. Finally, we predict the changes of EC and water levels in the BTL coastal aquifers for the near future by employing a time series algorithm.

2. Geology

The saline Bakhtegan-Tashk Lake (BTL) is located in southern Iran, 50 to 160 km north-east of Shiraz. Based on tectonic, magmatic and sedimentary features, this region is situated in the High Zagros Zone. The High Zagros Thrust Belt has a width of more than 80 km and is located between the Main Zagros Thrust and the High Zagros Fault in the southeastern part of the High Zagros Thrust Belt (Agard et al., 2005; Alavi and Mahdavi, 1994; Berberian, 1995). Most of the western, northern and southern parts of the study area comprise karst formations (Khaneh Kat, Neyriz, Surmeh, Fahiylan, Dariyan, Sarvak, Tarbur and Asmarijahrum) and the eastern and central parts comprise of the Ophiolitic rocks (Geological Survey of Iran, 2002). BTL and all coastal aquifers are located in Quaternary Alluvium deposits (Fig. 1) Details of the sedimentary sequence and the structural characteristics of this area are discussed by Stocklin and Setudehnia (1977).

3. Physiography and Hydrogeology

The area of the Bakhtegan and Tashk Lake is 850 and 410 Km^2, respectively. The Bakhtegan and Tashk Lakes are separated in dry years, but forms a single lake during heavy precipitation, about every 12 to 16 years. The catchment area of the BTL is 27180 Km^2.

With a maximum and minimum elevation of 2930 and 1545 above sea level, m. a. s. l, respectively. The climate of the BTL is arid with annual average, minimum and maximum precipitation of 232, 68, and 441 mm/y, respectively from 1968 to 2018. The average temperature and mean annual pan evaporation is 19 °C and 2749 mm/y, respectively. Precipitation mainly occurs from November to April.

The Kor River is the only permanent river that discharges into the BTL with an average discharge of 13.58 m^3/s from 1997 to 2007, but the average discharge decreased profoundly to 0.88 m^3/s since 2007, due to overexploitation, drought and construction of two new dams on the BTL catchment area (Fars Regional Water Authority (FRWA, 2016). The main water sources for Bakhtegan Lake (BL) are Kor River, a manmade drainage canal to the south of Kor River and numerous natural drainages around the lake. Sources for Tashk Lake (TL) are the Gomban Spring with a discharge of 0.716 m^3/s, a manmade drainage canal to the north of Kor River, an overflow of
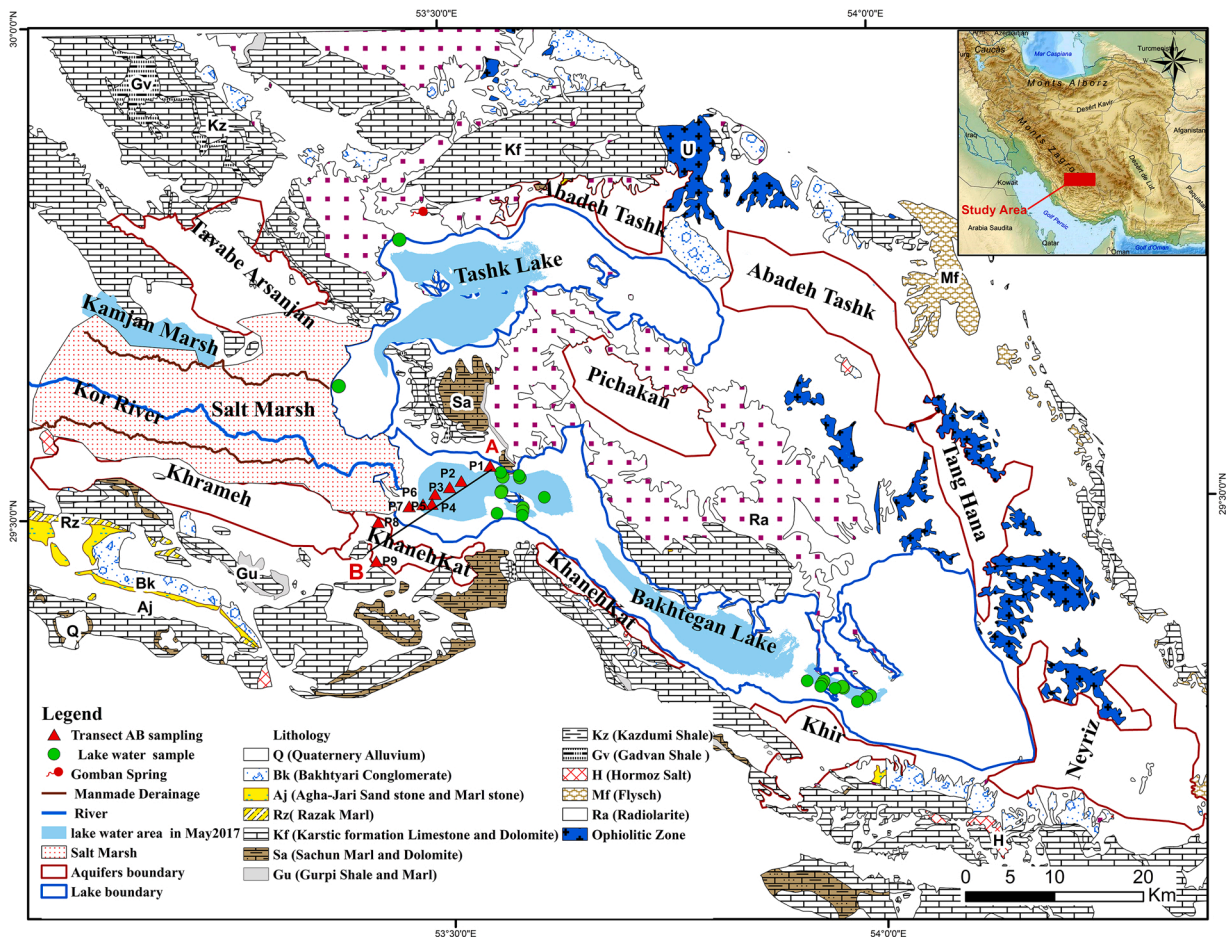

Fig. 1. Geological map of the study area (scale: 1/100000) and AB is sampling transect in Fig.5.

the Kamjan marsh and numerous natural drainages around the lakes.

The area of Kamjan marshes is about 100 km^2 with permanent and seasonal marshes along the Kor River, but the area of this wetland has decreased to 52 km^2 by rice farm since 1967.

Three dams, Doroudzan 1972, Mollasadra 2006, and Sivand 2006 have been constructed in the catchment area of the Kor River with a total effective capacity of 1285 MCM (Fars Regional Water Authority (FRWA, 2016)). Tens of diversion canals transfer the Kor River for agricultural purposes throughout its route. The lower part of the Kor River was diverted for agricultural purposes by six old diversion canal, but recently no water is diverted due to overexploitation in the upper parts of the basin. The oldest diversion dam is Band-e-Amir, which was constructed more than 1000 years ago (Torabi Haghighi and Kløve, 2017).

Six unconfined aquifers and a salt marsh are located around the BTL and two unconfined aquifers are in direct contact with the salt marsh (Fig. 1). These eight aquifers are referred to as coastal aquifers, as limestone aquifers are located upstream of the coastal aquifers. The characteristics of coastal aquifers are summarized in Table 1. The discharge of most coastal aquifers decreased in 2009 due to drought.

The eight unconfined alluvium aquifers are composed of sand with little clay close to the BTL or salt marsh boundary and it changes to young terraces at the highland consisting of gravel, sand, silt and clay (Geological Survey of Iran, 2002). The salt marsh is composed of silt and clay with evaporated salt. The salt marsh has a water table near the ground surface and there are no exploitation wells and agricultural land due to groundwater salinity. The texture of the BTL sediment was measured with hygrometry in several sites. The texture is mainly clay loam or sandy silty clay. The transmissivity ranges from 9 to 436 m^2/day and the specific yield varies from 0.021 to 0.1 (Fars Regional Water Authority (FRWA, 2009).

The recharge of coastal aquifers is mainly the result of direct precipitation, surface runoff, inflows from the upstream karstic aquifers and irrigation and industrial return flow. The coastal aquifers are only exploited by 3597 and 3280 wells with a total annual discharge of 441 and 411 MCM in 2004 and 2009, respectively (Table 1). Evaporation from the watertable is negligible because the depth to the water table exceeds 5 m in coastal aquifers. The thickness of the unsaturated zone in the coastal aquifers varies from 5 to 112 m mainly less than 50 m. Gomban karst spring naturally discharges into the Thask lake but its water mainly used for agricultural purposes since 30 years ago. The water budget of coastal aquifers in Tavabe Arsanjan, Abadeh Tashk, Khir and Neyriz were -19.53, -14.37, -12.64, -2.69 MCM, respectively wet year of 2004 due to over exploitation but Khanekat and Kharameh are at balance (Fars Regional Water Authority (FRWA, 2009).

4. Materials and methods

4.1. Data Collection

This study partly uses available data that were obtained from Fars Regional Water Authority (2009 and 2016). These data include coordinates, discharge, depth to the water table, depth of well and Electrical Conductivity (EC) for 3597 and 3280 exploitation wells of the coastal aquifers in 2004 and 2009, respectively. Chloride concentration was only measured for all wells in 2004 in the national inventory. In addition, major cations, anions, Total Dissolved Solids (TDS) and EC have been measured seasonally in 262 typical wells of the coastal aquifers from 2002 to 2018. The water level has been measured in 112 piezometers in coastal aquifers from 1992 to 2018 in Kharameh and Tavabe Arsanjan, from 1994 to 2018 in Neyriz, form 1996 to 2018 in Khir, form 2008 to 2018 in Abadeh Tashk, form 2009 to 2018 in Pichkan, Tang Hana, and Khaneh Kat.

The relationship between EC and TDS commonly used is

$$TDS(mg/l) = k_e \times EC(\mu S/cm) \tag{1}$$

where k_e ranges mostly 0.55 - 0.75 (Hem, 1985). The lower conversion factors (k_e) concern chloride-rich and higher k_e apply for sulphate-rich water. The value of $k_e = 0.65$ has been adopted by US Geological Survey (Rainwater and Thatcher, 1960; Hubert and Wolkersdorfer, 2015; Thorslund and van Vliet, 2020). Isopotential maps were constructed by ordinary kriging with a linear variogram

Table 1
General characteristics of eight coastal aquifers of the BTL (Fars Regional Water Authority (FRWA, 2009 and Fars Regional Water Authority (FRWA, 2016).

Aquifer name	Area (km^2)	Aquifer Thickness (m)	Transmissivity (m^2/day)	Specific yield (%)	No of wells 2004	Total discharge 2004 (MCM)	No of wells 2009	Total discharge 2009 (MCM)
Khane Kat	92.77	<10-75	NA	0.063	303	34.5	404	21.14
Khrameh	174.01	<10-200	9-1362	0.075	710	74.0	629	114.24
TavabeArsanjan	170.44	<10- 105	38.5-436.5	0.021	1610	118.2	808	50.73
Tange Hana	134.06	<10-40	61		117	19.15	135	16.21
Neyriz	191.32	<10-140	24-297.5	0.1	248	33.06	332	40.72
Abadeh-Tashk	287.45	<1-90	25.5-144	0.1	533	107.17	566	134.36
Khir	84.04	<10-90	41-76	0.1	237	45.57	247	24.55
Pichakan	70.55	<10-40	NA	NA	49	9.25	45	9.41
Total					3597	440.99	3280	411.36

NA: not available

in the spatial analyst toolbox of ArcGIS.

4.2. The salinity of BTL, salinity and hydraulic head along cross section A-B

After heavy rain in the early spring of 2017, the flood water mainly filled the deep parts of the lake. A total of 23 surface water samples of BTL were collected to measure TDS from May to June 2017 (Fig. 1 and Table 2). To determine the flow direction and salinity gradient from lake to a typical coastal aquifer, seven piezometers were constructed inside the BTL and part of Khane Kat aquifer (cross section A-B in Fig. 1). Water samples were collected and depth to water table and elevation of ground surface were measured in 2 piezometers in the Khane Kat aquifer and 7 piezometers inside the lake in October 2018 (Fig. 5). The samples were analyzed for the major ions and total dissolved solids (TDS) at the Hydrochemistry Laboratory of the Department of Earth Sciences, Shiraz University, Iran. Calcium (Ca^{2+}) and magnesium (Mg^{2+}) were measured by titration with EDTA (ethylene diamine tetra acetic), using Murexide and Erichrom Black-T as indicators. Sodium (Na^+) and potassium (K^+) concentrations were determined by the standard F-AAS method. Chloride and Sulfate (SO_4^{2-}) concentrations were measured by Mohr and turbidity methods, respectively. Bicarbonate (HCO_3-) was determined by titration with HCl using methyl orange as an indicator. TDS values were measured by the evaporation method. For quality control measures, the ionic balance error was calculated as follows:

$$Ionic\ balance\ error\ (\%) = \frac{\Sigma Cations\ (meq) - \Sigma Anions\ (meq)}{\Sigma Cations\ (meq) + \Sigma Anions\ (meq)} \times 100 \qquad (2)$$

The calculated error did not exceed 5.8%. The TDS at the lakeside is significantly higher than the land side of Transect AB, resulting in different water density. Therefore, water level of the piezometers must be corrected for the density differences as follow:

$$\rho_s = \rho_f + \frac{\partial \rho}{\partial C} C, \qquad (3)$$

Where ρ_s is the saltwater density with elevated salt concentration C, ρ_f the freshwater density, and the slope $\frac{\partial \rho}{\partial C} = 0.7143$ for the range from freshwater to seawater (Langevin et al. 2003).

$$E_c(x) = (E(x) - 1534.05).\rho_s(x) + 1534.05 \qquad (4)$$

Where 1534.05 m is the lowest water level (with salt-free water), E_c is the corrected water table, E is measured water table in the field at position x.

4.3. Water type and percentage of lake water intrusion

The geochemical evolution of groundwater and pathways of fresh and saline water movement may benefit from plotting the concentrations of major cations and anions in the Piper tri-linear diagram. Piper diagram has been divided into six subcategories: (1) Ca–HCO$_3$ type, (2) Na–Cl type, (3) mixed Ca–Mg–Cl type, (4) mixed Ca–Na- HCO$_3$ type, (5) Ca–Cl type, and (6) Na–HCO$_3$ type. The groundwater types of the study area were distinguished and grouped by their position on the Piper diagram where concentration is assigned in % of meq/l (Piper, 1944).

Processes controlling water chemistry were assessed using the Gibbs diagram (Gibbs, 1970), where groundwater was plotted in between the two end members; rain water, represents the main recharge source for groundwater and lake water represents the source for groundwater salinization. Inference that can be made from this plot includes that groundwater has been affected largely by lake water mixing and partially by the water-rock interaction.

Lake water fraction (f_{lake}) is quantified using the chloride concentration as this ion is considered to be a conservative tracer, not affected by rock/water interactions and it is calculated as follows (5) (Appelo and Postma, 2005):

$$f_{lake} = \frac{C_{cl,sample} - C_{cl,fresh}}{C_{cl,lake} - C_{cl,fresh}} \qquad (5)$$

where $C_{Cl,sample}$ is the Cl- concentration of the sample, $C_{Cl,lake}$ is the average Cl- concentration of the BTL and $C_{Cl,\ fresh}$ represents the lowest Cl- concentration of the freshwaterzone.

Table 2
TDS (mg/l) of the BT and TL before shrinkage (previous studies) and after shrinkage.

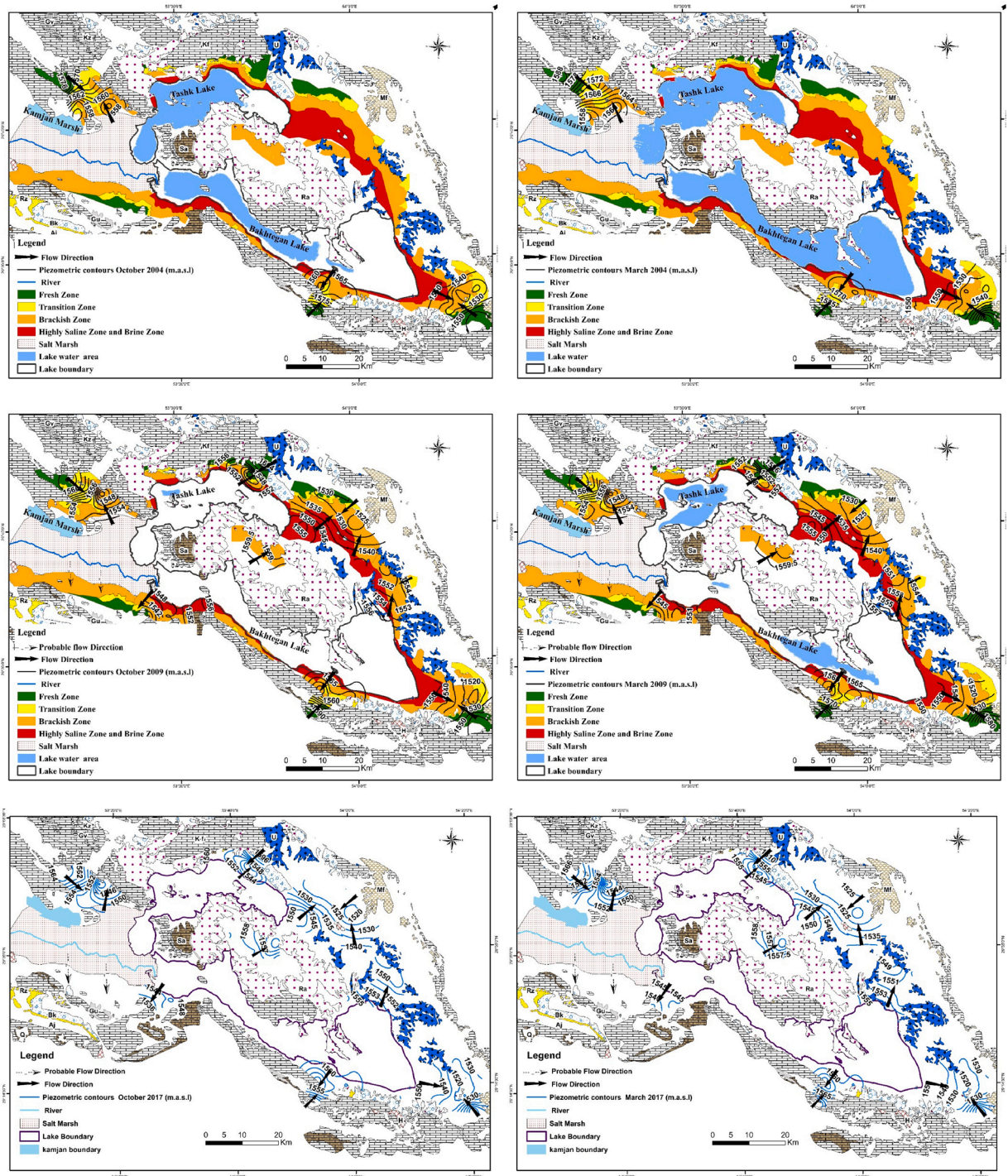| Date		TDS before Shrinkage		TDS after shrinkage	
		1959	1994	2007	2017
Reference		Loffler, 1961	Nejati, 1994	Agh, 2007	this study
Bakhtegan Lake	min	12810		60000	200000
	max	90300		250000	451500
Tashk lake	min	43400	31200		73300
	max	60550	45400		128000
	Total Average		45400		256000

Fig. 2. (a) Spatial distributions of EC using 2415 exploitation wells, Iso-potential lines and general flow direction of the coastal aquifers in October 2004 (left map) and March 2004 (right map). Geological legend presented on Fig. 1. (b) Spatial distributions of EC based on 2296 exploitation wells, Iso-potential lines and general flow direction of coastal aquifers wells in October 2009 (left map) and March 2009 (right map). Geological legend presented on Fig. 1. (c) Iso-potential lines and general flow direction of coastal aquifers in October 2017(left map) and March 2017 (right map). Geological legend presented on Fig. 1.

4.4. Forecasting model

Support Vector Regression (SVR) approach concerns regression of the type of Support Vector Machines (SVM), a machine learning algorithm based on statistical learning theory proposed by Vapnik (1995). SVR is one of the most popular techniques for environmental time series analysis and prediction based on past observations (Shiri et al., 2013; Ahmadianfar et al., 2020; Phan and Nguyen, 2020). SVMs can be used for classification or regression problems that are not linearly separable by transforming original data into a new space using Kernel functions.

Various types of kernel functions such as the radial basis function (RBF), the linear, sigmoid, polynomial (Poly) and exponential radial basis function (ERBF), can be applied in SVM.

The SVM regression estimating function can be described as:

$$F(x) = w\varphi(x) + b \tag{6}$$

where w is the weight vector, φ is a nonlinear transfer function mapping the input space into a high-dimensional feature space, b is the bias and x is the input vector.

In this study, a nonlinear SVR is used to forecast the water level and EC for the period 2018–2026 based on the water level and EC values measured from 2002 to 2018 in the BTL coastal aquifers. The poly kernel function and the different lag length was employed by trial and error procedure to give the best simulation result.

4.4.1. Forecasting accuracy evaluation

The accuracy SVR was evaluated by correlation coefficient (R^2), Root Mean Square Error (RMSE), Mean Absolute Percentage Error (MAPE), and Mean Absolute Error (MAE), which can be expressed using the following equations.
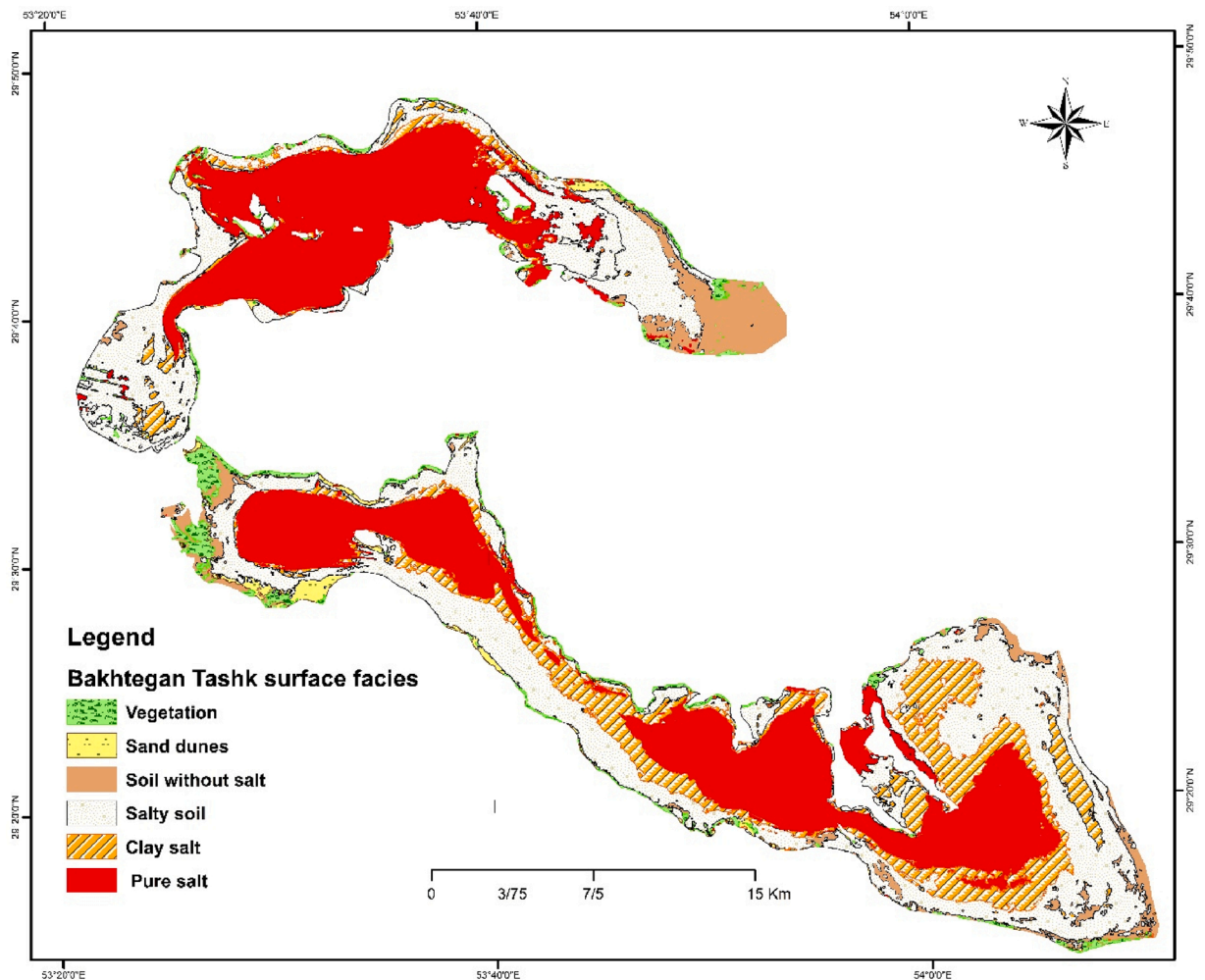

Fig. 3. Surface facies of the Bakhtegan and Tashk lakes after Mohammadi (2020).

$$R = \sum_{i=1}^{n} \frac{\left(O_i - \overline{O}\right)\left(P_i - \overline{P}\right)}{\sqrt{\sum_{i=1}^{n}\left(O_i - \overline{O}\right)^2 \sum_{i=1}^{n}\left(P_i - \overline{P}\right)^2}} \tag{7}$$

$$MAPE = \frac{1}{n}\left|\sum_{i=1}^{n}\frac{O_i - P_i}{O_i}\right| \times 100 \tag{8}$$

$$RMSE = \sqrt{\frac{1}{n}\sum_{i=1}^{n}(O_i - P_i)^2} \tag{9}$$

$$MAE = \frac{1}{n}\sum_{i=1}^{n}|(O_i - P_i)| \tag{10}$$

where O_i is the ith observation value for EC or water level, P_i is the ith forecasted value for EC or water level; $\overline{O}$ and $\overline{P}$ stand for the mean observed and forecasted EC or water level, respectively; and n is the total number of data samples evaluated. The observed and forecasted results were compared to select the best forecasting model.

5. Results and discussion

5.1. EC of the coastal aquifers

The EC of the coastal aquifers in 2004 and 2009 are presented in Fig. 2a and b using the national inventory data. The isopotential maps of 2004 (wet year), 2009 (dry year) and 2017 (wet year) for dry month (October) and wet month)March(presented in Fig. 2a, b and c, respectively based on available data. The isopotential maps of Khane Kat, Abadeh Tashk, Pichakan, and Tang Hana aquifers were not presented in Fig. 2a, because piezometers were constructed after 2004. The EC of the coastal aquifers usually ranges from 160 to 20,000 μS/cm (Fig. 2a and b.). Taking into account that the EC of seawater is 45,000 μS/cm, these values indicate severe salinization of groundwater. The Cl data are only available in 2004, when chloride varied from 1 to 8,900 mg/l in 2004. The discharge ranges from 0.5 to 50 l/s. The TDS of brine sampling points along the cross- section A-B (as shown in Fig. 1) ranges inside the BL from 162000 to 363000 mg/l outside the lake from 600 to 10300 mg/l.

5.2. Salinity sources of lakes and coastal aquifers

There are few hydrochemistry data in the BTL. The results of previous studies indicate the average TDS of BTL was 45400 mg/l before shrinkage in 2007, but it has increased to average 256000 mg/l, since 2007 (Table 2). The BTL is classified into 5 facies based on surface crust namely pure salt, clay salt, salty soil, soil without salt and sand dune from center of the lake toward its shoreline, respectively (Fig. 3). The BTL water evaporates and salt is deposited in deeper parts of the BTL which receives more water than shallow parts. The soil without salt facies is located close to shoreline, it was rarely covered by water and has the largest depth of the water table. The source of salinity before shrinkage under natural condition is evaporation from the BTL water. When the lakes get dry, the evaporation occurs from saline water below the lakes bed in deeper parts of the BTL where depth to the water table is shallow. The pure salt facies in the deep parts of BTL are exposed during dry periods and redissolved in case of rainfall or floodwater.

The following reasons cause the BTL salinity:

1 The average rainfall on the BTL area is about 232 mm but annual class pan evaporation is about 2749 mm/yr.
2 The main resources of the BTL water are Kor River and the Gomban spring with a total annual inflow of 428 and 22.6 MCM with an average EC of 2415 μS/cm and 5260 μS/cm respectively, therefore these two water resources are not the BTL salinity sources.
3 The salt marsh is a lowland area with a shallow water table. The EC of salt marsh was between 100000 to 150000 mg/l near the BTL and it decreases away from the BTL (toward the west) (Rezaei, 1998), but no more data is available. The source of the BTL salinity is not salt marsh because the salt is deposited in the deep parts of BTL, even 50 km far from the Salt Marsh (Fig. 3). The salt marsh may be partly a source of saltwater in the adjacent lakes area, but it merits more research.

The main reasons for the increasing salinity since 2007 are reduction of the BTL inflow due to drought, construction of two dams in the BTL catchment area that limit inflow in BTL, and over-exploitation in the aquifers of BTL catchment area and coastal aquifers. After shrinkage of the lake, the main sources of BTL water are precipitation onto the lakes and natural drainage. BTL water completely evaporated during dry months after shrinkage. Dissolution of salt in salty facies during the wet season is another source of salinity.

Salinity sources of the coastal aquifers are BTL and salt marsh. Tavabeh Arsanjan and Kharameh coastal aquifers are in direct contact with salt marsh and the rest of the coastal aquifers are in direct contact with BTL (Fig. 1). The salinity source of the Pichakan, Tang Hana, Khane Kat, Neyriz, Khir and Abadeh Tashk aquifers are the BTL for the following reasons:

1 They are in direct contact with the BTL.

2 The TDS of piezometers inside the BTL ranges from 162000 to 363000 mg/l in 2017 (Fig. 5) and the average TDS after shrinkage significantly increased (Table 2).

3 The EC has the highest value near the BTL Boundary and it decreases toward the high lands (Fig. 2a and b).

4 The depth to the water table in all coastal aquifers was more than 5 m, therefore, evaporation of groundwater by capillary rise from the water table was not the source of coastal aquifer salinity. Evaporation from the water table is insignificant if the water table is more than about 3 m below the soil surface (Van Der Zee et al., 2014).

5 In addition, the unit hydrographs (mean area-weighted water level of piezometers) of most coastal aquifers have a negative trend since 1992 or 2009 (Fars Regional Water Authority (FRWA, 2018) (Fig. 4), due to overexploitation, increasing the hydraulic gradient toward the coastal aquifer.
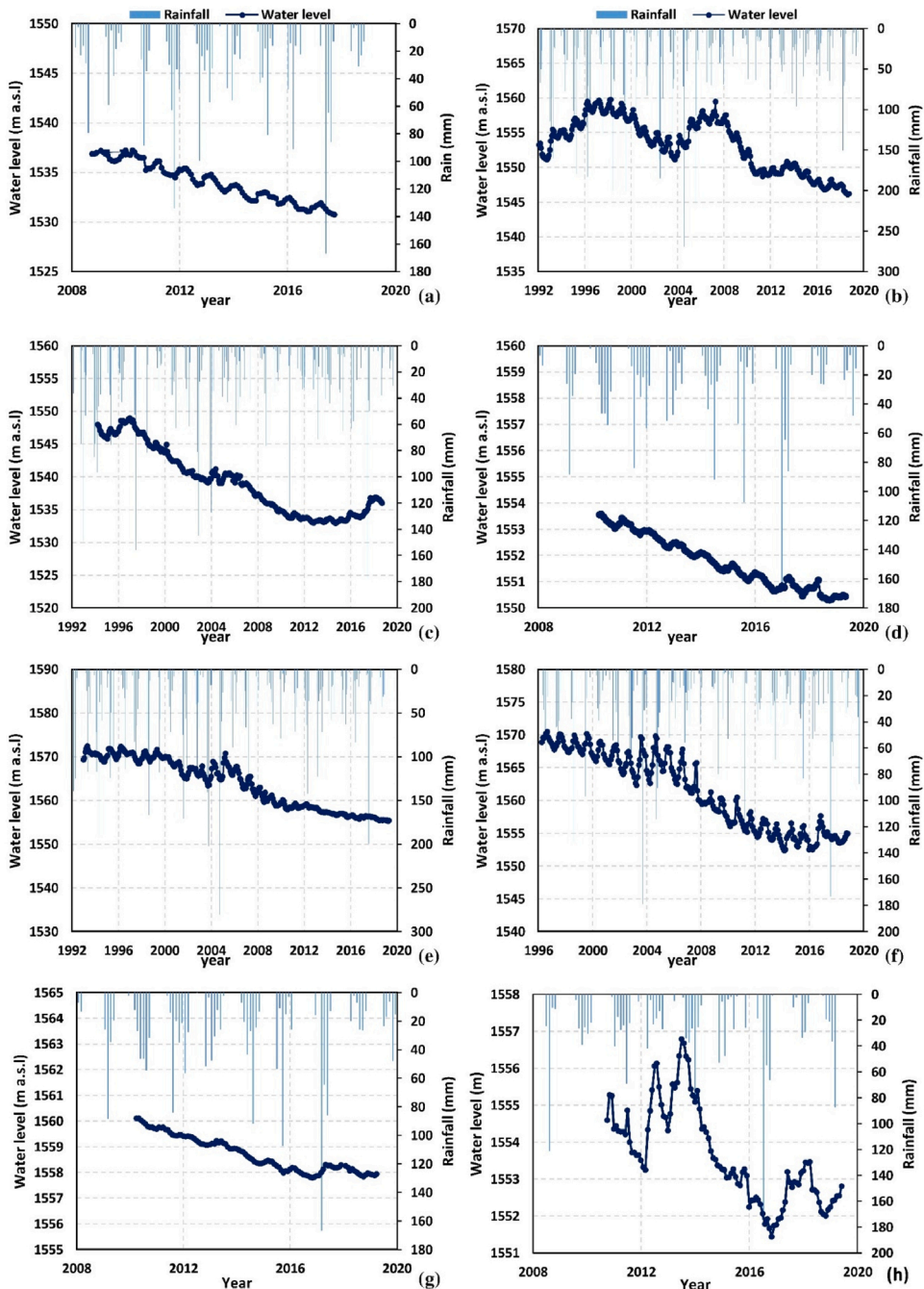

Fig. 4. Long term unit hydrographs (mean area-weighted water levels of piezometers) of coastal aquifers: (a) Abadeh Tashk aquifer, (b) Kharameh aquifer, (c) Neyriz aquifer, (d) Tang Hana aquifer, (e) Tavabe Arsangan aquifer, (f) Khir aquifer, (g) Pichkan aquifer, and (h) Kaneh Kat aquifer.

6 The geological formations in the study area are karstic limestone and low permeability, Radiolarite and Ophiolite rocks without any salt origin.

7 The intrusion of saline water into the coastal aquifer is a common process in the saline lakes (Delsman et al., 2014; Kazakis et al., 2016; Argamasilla et al., 2017; Khadra et al., 2017; Mahlknecht et al., 2017; Abu-alnaeem et al., 2018).

The sources of Tavabeh Arsanjan and Kharameh coastal aquifers are most probably the salt marsh because EC decreases from the salt marsh toward the highland (Fig. 2a and b). The general flow direction is from the boundary between the salt marsh and Tavabeh Arsanjan aquifers toward the highland in wet and dry seasons (Fig. 2). There are a few scattered piezometers along the length of Kharamah aquifer, therefore, it is not possible to plot iso-potential maps. There are no piezometers inside the salt marsh during this study period, which merits a closer investigation of salt marsh. In addition, items 4 to 7 that justify the sources of salinity for the BTL, are also valid for these two aquifers.

5.3. Groundwater flow in the coastal aquifers

The natural flow direction used to be from karstic formations and coastal alluvium aquifers toward the BTL. Currently, however, it is directed from the BTL toward the coastal alluvium aquifers due to over-exploitation, as is apparent from the iso-potential maps of 2004, 2009 and 2017 for March and October (Fig. 2a, b and c). In addition to the iso-potential map presented in Fig. 2, extra iso-potential maps were prepared in 1996 for May, March and October, in 2004, 2009 and 2017 for May and in 2018 for May, March and October, they are presented in Figs. S1a, S1b, S1c, S1d and S1e. All of these iso-potential maps show the flow direction from the BZ toward the highland far from the BTL and Salt Marsh. It can be concluded that the flow direction is from the BTL and Salt Marsh in wet and dry periods.

The equivalent freshwater level in piezometers along cross section A-B (transect indicated in Fig. 1) is calculated using the density of pore water by Eq. (3) and (4) (Fig. 5). For seawater, $\rho_s = 1.025$ g/cm^3, but for the BTL, both salinity and density can be larger than that, and the density may increase even up to $\rho_s = 1.259$ g/cm^3. Accordingly, the corrected elevations show an even more pronounced gradient towards the land side. Due to the higher ρ_s also, wider mixing zones were found for 'active' SWI (Badaruddin et al., 2017). The slope of the water table, both corrected and not corrected with Eq. (4), indicates flow from the lake center towards the coastal alluvium aquifer. This indicates active SWI in the BTL aquifers.

The observations made in piezometers of cross section A-B (transect indicated in Fig. 1) show that the water level is highest in the center of the lake (Fig. 5). At this central position, the highest TDS (363,000 mg/l) is found at depth of 5 cm, which indicates the effect of intense evaporation fed by a capillary rise from the saltwater level. Moving from the center of lake towards the coast, the water level declines (depth to water table 2.5 m) and the concentration of TDS decreases to 162,000 mg/l. In part, this will be due to insignificant replenishment of evaporated water as capillary rise from the saltwater becomes insignificant if it is more than about 3 meters below soil surface (Van Der Zee et al., 2014).

5.4. Classification of the BTL coastal aquifers

Based on previous studies, groundwater is classified in five groups, (a) fresh, (b) slightly saline or brackish, (c) moderately saline or brackish highly saline (d) Highly saline, heavily saline or very saline (e) seawater or brine (Robinove et al., 1958; Winslow et al., 1968; Freeze and Cherry, 1979; Rhoades et al., 1992; Reese, 1994; Yobbi, 1996; Bureau of Reclamation, 2003; National Ground Water Association, 2010; Meyer et al., 2011; Stanton et al., 2017). In this study, the groundwater is classified into five major groups namely fresh, transition, brackish, highly saline and brine. The EC limits of each group is determined based on groundwater salinity beneath

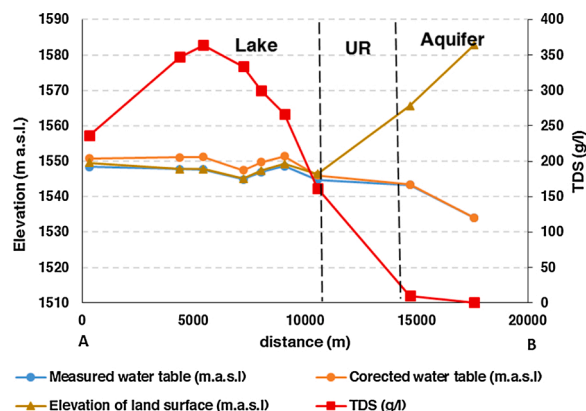**Fig. 5.** Total dissolved solids (TDS), measured and corrected water level in the piezometers, and elevation of land surface along the cross section A-B in October 2018 (indicated in Fig. 1). First vertical line represents boundary between the lake and the Unexploited Region (UR). This region is the area adjacent to the lake without any exploitation wells. The second vertical line represents boundary between the UR and coastal aquifer.

Table 3

Range, Average and No. of well of chemical and physical data for the Brackish Zone (BZ), Transition Zone (TZ) and Fresh Zone (FZ) in 8 coastal aquifers for 2004 and 2009.

Aquifer	zone		EC (μS/cm) 2004	2009	Cl (mg/l) 2004	2009	Saturation thickness (m) 2004	2009	Discharge(l/s) 2004	2009	General direction of flow	Water type
		Range	320 - 1290	500 - 1400	2.9 - 106.5		0.5 - 90	0.7 - 36.8	2.5 - 47	2.5 - 47.7		
Neyriz	FZ	Ave	(800)	(822)	(51.06)		(28.2)	(6.7)	(12.4)	(10.3)	Lake ward	HCO$_3^-$
		No. of well	31	76	19		35	59	52	88		
		Range	1040- 4392	1010 - 4300	106.5 - 710		1-60	0-27.3	2-19.7	0.5 - 17.5		
	TZ	Ave	(1900)	(1880)	(280)		(8)	(4.4)	(7.2)	(6.64)	Mixed	SO$_4^{2-}$, Cl$^-$
		No. of well	48	68	34		26	70	85	75		
		Range	2007 - 17633	2100 - 19500	248 - 6390		2.8 - 21	0.4 - 90.5	1.5 - 25	0.3 - 28.8		
	BZ	Ave	(6037)	(9430)	(1980)		(3.7)	(3.5)	(8.2)	(7.08)	Land ward	Cl$^-$
		No. of well	64	149	31		85	169	107	166		
		Range	920 - 1440	648 - 701					6 - 46	8.3 - 28.2		
Khir	FZ	Ave	(1320)	(670)					(22.4)	(15.7)	Lake ward	HCO$_3^-$
		No. of well	7	7					13	7		
		Range	1900 - 4050	1200 - 3910	177 – 639		10 - 29.9	0 - 37	2.5 - 45	3 - 28.1		
	TZ	Ave	(2370)	(2480)	(400)		(18.8)	(7.7)	(14.5)	(11.5)	Mixed	SO$_4^{2-}$, Cl$^-$, HCO$_3^-$
		No. of well	22	56	12		6	20	54	59		
		Range	2850 - 18740	2038 - 17150	461 – 4721		.5 - 41.2	1-30	1.5-25.5	1 - 25.6	Land ward	
	BZ	Ave	(6490)	(6999)	(1510)		(6.5)	(6.67)	(7.5)	(5)		Cl$^-$
		No. of well	50	179	34		71	175	166	180		
		Range	510 - 850	500 - 1300	11.8 - 92.9			3 - 49.2	3 - 22.1	2.9 - 25		
Khane Kat	FZ	Ave	(688)	(769)	(48.9)			(27.05)	(14.86)	(11.26)	Lake ward	HCO$_3^-$
		No. of well	8	14	3			4	23	18		
		Range	1055 - 3130	1091 - 3370	138.4 – 887		1 - 60	1 - 20	3.5 - 22	1 - 27.5		
	TZ	Ave	(1883)	(2110)	(384.2)		(11.42)	(17.56)	(11.94) 46	(5.45)	Mixed	Cl$^-$
		No. of well	12	21	6		20	41		51		
		Range	2350 - 11690	2320-16920	745.5- 4437		0.5 - 66	0.1 - 25	2.5 - 29	.5 - 22.5		
	BZ	Ave	(6887)	(6977)	(2012)		(7.73)	(5.4)	(7.83)	(4.5)	Land ward	Cl$^-$
		No. of well	48	142	43		196	379	238	333		
		Range		711-1630	24-70		13-29.5	3.8-90	3-15.5	5.5-23		
Khrameh	FZ	Ave		(1015)	(47)		(21.25)	(37.2)	(11.53)	(14.93)	Lake ward	HCO$_3^-$
		No. of well		21	2		2	42	51	42		
		Range	1507-1847	1300-3700			14-30	11.5-63	3 - 16	4.92-23		
	TZ	Ave	(1677)	(2693)			(21.3)	(35.82)	(11. 3)	(14.42)	Mixed	Cl$^-$
		No. of well	2	11			3	32	31	36		
		Range	3112 - 19400	2100-14200	216.5 – 4615		1.1 – 35	2-79	1.5 -16.5	5-60		
	BZ	Ave	(9846)	(6525)	(1463)		(12)	(18.79)	(10.8)	(13.51)	Land ward	Cl$^-$
		No. of well	10	51	18		74	330	313	373		
		Range	920-2000	400 – 2300	62.1- 198		0.5 - 63	0.8 -90	3 - 50	0.5 - 16.5		
Tavabe Arsanjsn	FZ	Ave	(1258)	(1040)	(136.4)		(13.5)	(14.7)	(8.72)	(4.7)	Lake ward	HCO$_3^-$
		No. of well	317	246	80		232	81	401	268		
		Range	1300 - 8700	1300 - 8300	156-1490		0 - 186	0.5 - 90	61 - 42	0.5 - 37.5		
	TZ	Ave	(3040)	(3010)	(611)		(15.1)	(10.1)	(8.72)	(7.3)	Mixed	Cl$^-$
		No. of well	632	385	96		346	246	734	395		
		Range	3180- 36662	3000 - 14450	1011 - 8875		15 - 166	0.1 - 90	1.5 - 45	1.5 - 45		
	BZ	Ave	(8620)	(7330)	(2630)		(12.4)	(5.87)	(6.9)	(6.8)	Land ward	Cl$^-$
		No. of well	526	235	58		390	245	585	493		
		Range	450 - 1160	400-1224	24.9 - 74.6		2 - 30.3	0.5 - 233	.5 - 50	1.2 - 50		
Abadeh Tashk	FZ	Ave	(655)	(584)	(24.9)		(14.1)	(13.2)	(19.9)	(17.2)	Lake ward	HCO$_3^-$
		No. of well	91	119	4		20	127	97	116		

Table 3 (*continued*)

	TZ	Range	1330 - 3390	1300- 4000	163.3 -287.5	1.5 - 32.1	0.5 - 40	1 - 50	2.7 - 43.2		
		Ave	(2019)	(2828)	(214.6)	(9.3)	(7.4)	(19.1)	(16.5)	Mixed	Cl⁻
		No. of well	101	77	3	40	88	105	94		
	BZ	Range	2150 - 19590	2420 - 18950	237 - 5058	1.2 - 20.5	0.2 - 40	1 - 43	1.5 - 46.5		
		Ave	(7646)	(9340)	(2515)	(8.4)	(4.9)	(12.4)	(12.9)	Land ward	Cl⁻
		No. of well	307	290	17	52	305	330	305		
Pichakan	BZ	Range	3700- 13000	3420 - 19450	710 - 3461	1.7 - 8.6	0.3 - 90	3 - 42	4 - 27		
		Ave	(8060)	(9640)	(2307)	(5.15)	(4.84)	(15.9)	(11.7)	Land ward	Cl⁻
		No. of well	44	43	15	12		49	45		
Tang Hana	TZ	Range	1200 -3600	1845 - 2950	117-284	12-39	1 - 76	8 - 23	6 - 20		
		Ave	(2300)	(2594)	(200.3)	(26.5)	(11.4)	(16.4)	(12.9)	Mixed	Cl⁻
		No. of well	5	6	2	3	10	7	10		
	BZ	Range	2850- 14820	3270 - 19450	149 - 4836	1-26.5	0.3 - 10.7	4 - 42	1.5 - 22		
		Ave	(8520)	(10250)	(2494)	(10.1)	(1.72)	(12.8)	(9.16)	Land ward	Cl⁻
		No. of well	90	121	16	20	126	110	126		

the BTL and coastal aquifers. All of the coastal aquifers comprised of Brine Zone (BrZ), Highly Saline Zone (HSZ), Brackish Zone (BZ), and Fresh Zone (FZ), and Transition Zone (TZ) based on EC values, and considering other parameters such as Cl concentration, water type, and aquifer saturation thickness in each zone (Table 3) except Pichakan and Tang Hana aquifers. Pichakan and Tang Hana aquifers have a vast brackish zone because they are in direct contact with impermeable Radiolarite and Ophiolite rocks, respectively (Fig. 1) and there are no sources of freshwater to form FZ. The boundary of each zone is defined using the EC changes, instead of the chloride concentration, because EC was measured in all wells in 2004 and 2009, but chloride concentration was only measured in typical wells and only in 2004. The EC values of Khane Kat and Neyriz in 2009 and area of each zone are presented in Fig. 6. The other coastal aquifers have the same trend and behavior. The unexploited region from the BTL shoreline to the boundary of agricultural land consists of the BrZ and HSZ. The TDS along the transect AB is 363,000 mg/l at the center of the lake, and it gradually reduces to 162,000 mg/l at the BTL shoreline (Fig. 5).

The first part of the unexploited region, adjacent to the shoreline is brine, confirming active salt water intrusion. The EC reduces along the unexploited region due to precipitation recharge and reduction of the capillary fringe due to the enhancement of water table depth. The salinity of BrZ and HSZ is at such a level that no plants can survive. There is no EC data in unexploited region to determine the boundary between the BrZ and HSZ. The schematic boundary between these two zones is presented in Fig. 6. The BZ is from the end of HSZ to the beginning of TZ and the type of water is chloride. The BZ is located above the interface of this zone with the underlying HSZ. The EC at the beginning of BZ ranges mostly from about 15,000 to 20,000 μS/cm at different coastal aquifers (Table 3). The unexpected high range of EC at beginning of the BZ (near the boundary of HSZ and BZ) is due to high discharge rate of pumping, deepening some of the exploited wells, short distance to neighboring wells, and type of crops (halophytes). The high range of EC may result in significant reduction of crops yields. The quality of groundwater gradually increases in the BZ, due to precipitation recharge and agricultural return flow. In addition, the depth to interface between the HSZ and BZ increases along the BZ and, consequently reduces the effect of HSZ diffusion on salinity of the BZ. TZ is mixing of brackish and freshwater. The source of freshwater is alluvium or karstic aquifers at the high land around the BTL which flow toward the TZ. The boundary between the BZ and TZ is determined by a sharp and significantly high reduction of EC on both sides of this line (the red color line on Fig. 6). It implies that saltwater intrusion is stopped in the TZ. In the TZ, EC ranges from 1,100 to 4,300 μS/cm. The found boundary is also found by the sharp Cl concentration difference on opposite sides. The boundary between the TZ and the FZ is slightly arbitrary, but still well defined by the change of EC > 1,200 μS/cm in the TZ to EC < 1200 μS/cm for the freshwater zone (Fig. 6). Average of EC in the beginning and end of each zone of the BTL coastal aquifers shows the same trend as Khane Kat and Neyriz aquifers except Pichakan aquifer, because BZ of this aquifer is surrounded by the HSZ and there is no fresh aquifer (Fig. 7).

As was mentioned earlier, based on long term investigation of iso-potential map the general flow direction is from both the BZ and FZ toward the TZ (except Pichakan and Tang hena) in wet and dry years and months (Fig. 2a and b). In addition, The TZ is usually narrow in most of the coastal aquifers. The EC and Cl concentrations in the FZ are less than 1200 μS/cm and 100 mg/l, respectively. The water type in this zone is of the bicarbonate type. The general flow direction is from the karstic formation toward the alluvial aquifers. These classes imply that the concentration and EC range of the three zones show a region of common overlap. Because for all 8 aquifers, the local conditions are quite complex: besides active SWI, as a process that controls the distribution of salinity, also extractions at many places and diverse depths and rates affect the salinity distribution in the vertical direction (e.g., due to upconing). Spatial distribution of EC in the maps for 2004 and 2009 (Fig. 2a and b) indicates that in the parts of aquifers closest to the lake the highest EC values are measured and with increasing distance from the lake, the EC-values reduce. The progression of active SWI in the BZ is different in the different coastal aquifers. The Pichakan and Tang Hana aquifers, which are surrounded by impervious Ophiolite and Radiolarite rocks, do not experience a freshwater recharge towards the alluvial aquifers. This leads to a larger intrusion, and
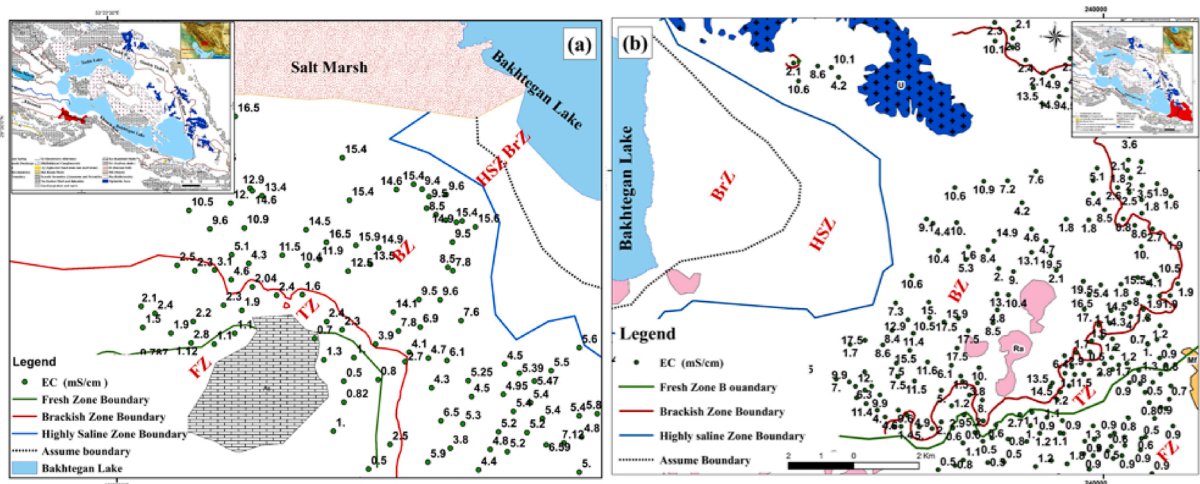

Fig. 6. The schematic area of Brine Zone (BrZ), Highly Saline Zone (HSZ), Brackish Zone (BZ), Transition Zone (TZ) and Fresh Zone (FZ) based on the EC values (a) Khane Kat aquifer (b) Neyriz aquifer.
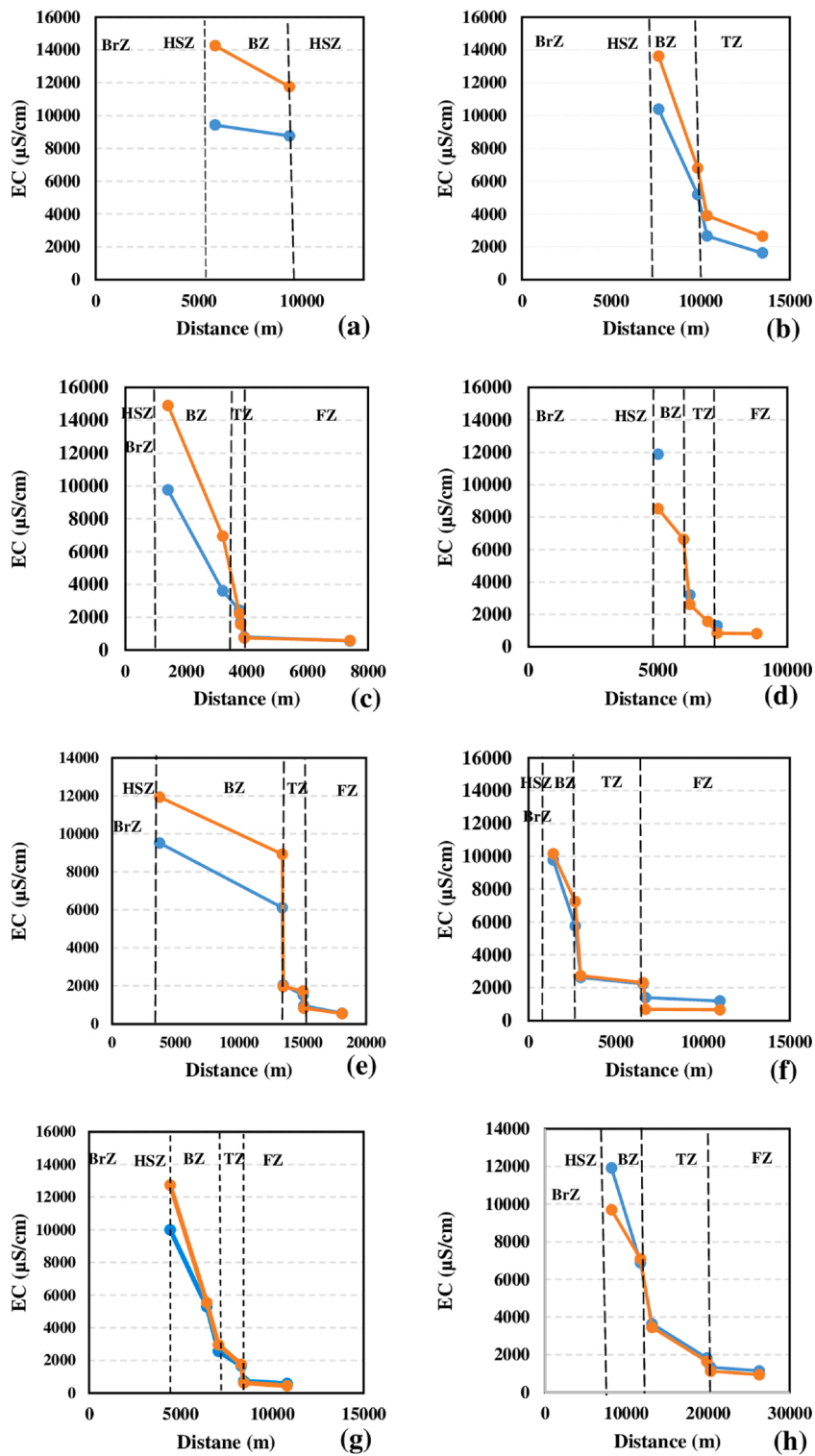
Fig. 7. Average of EC in the beginning and end of each zone of the coastal aquifers. Distance zero representing the lake boundary in Fig. 1. (a) Pichakan aquifer, (b) Tang Hana aquifer,(c) Khane Kat aquifer, (d) Kharameh aquifer, (e) Neyriz aquifer, (f) Khir, (g) Abadeh Tashk, (h), Tavabe Arsangan aquifer. Brine zone (BrZ), Highly saline zone (HSZ), Brackish Zone (BZ), Transition Zone (TZ) and Fresh Zone (FZ). EC data 2004 and 2009 represent blue and red line respectively.
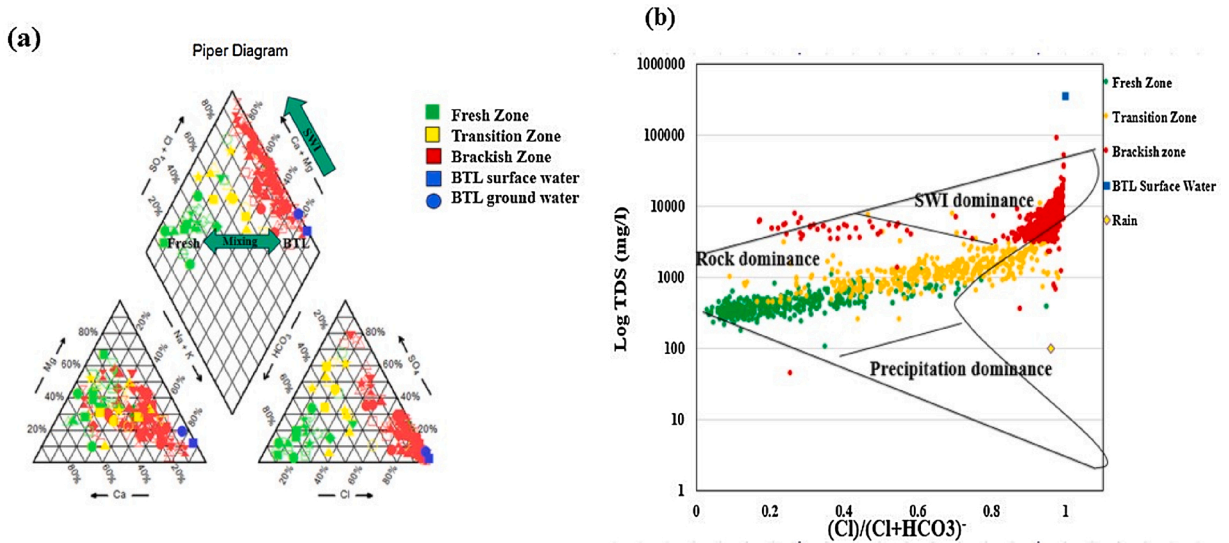
(a)

(b)

Fig. 8. (a). Piper diagram characterizing water types and chemical behaviors in the study area. And (b). Gibbs plot that illustrates the gradual change of salinity and chemical water composition from freshwater to lake water from 2002 to 2018.

farther extension of the BZ. By comparison of the spatial distribution of EC maps in 2004 and 2009, it is apparent that the regions with EC values exceeding 10,000 μS/cm incased in 2009, which is far more than in 2004. Due to BTL shrinkage, the increase of the density of the lake water and the drop in the water table by over-exploitation and dry years lead to increasing EC in the aquifers.

5.5. Hydrochemical variation

Using Eq. (2), lake water fractions range from 0.0 to 5.1% in the all coastal aquifers. The low lake water proportion within the FZ indicate that these regions are not affected by active SWI. In contrast, the highest lake water proportion is found in the BZ indicating that this zone is more vulnerable to lake water intrusion. The lake water proportion of groundwater increases towards the lake. Besides
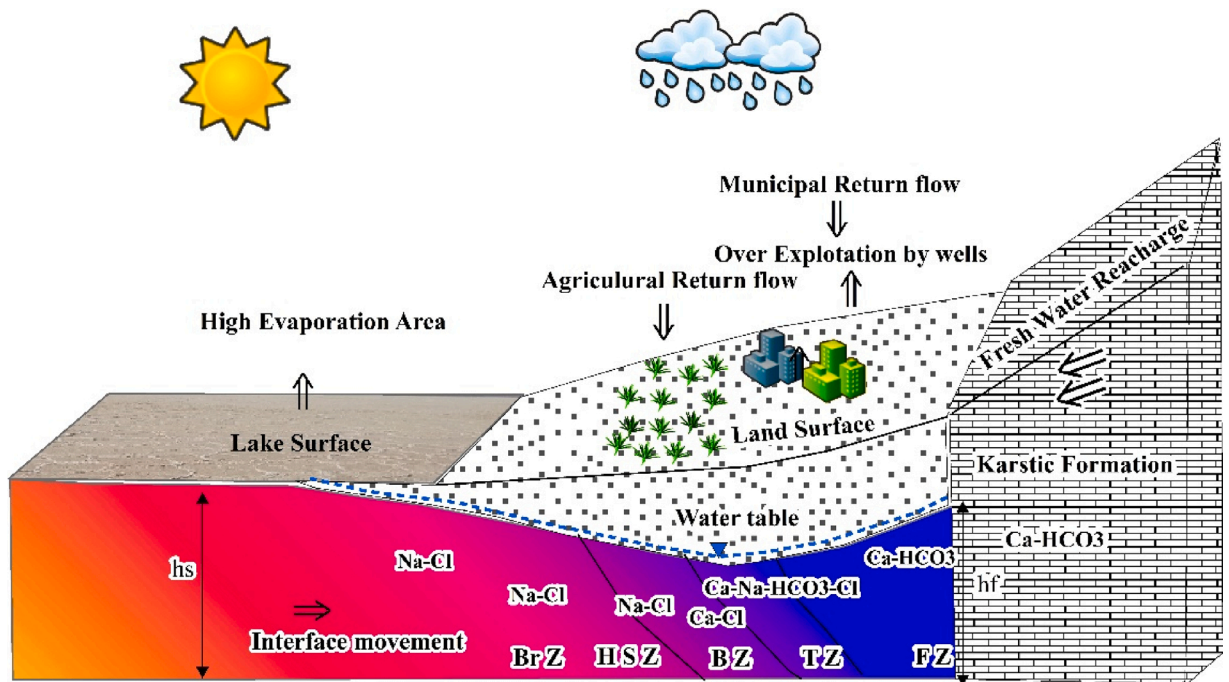

Fig. 9. Conceptual schematic of active SWI of coastal aquifers: Brine zone (BrZ) Highly saline zone (HSZ), Brackish Zone (BZ), Transition Zone (TZ) and Fresh Zone (FZ).
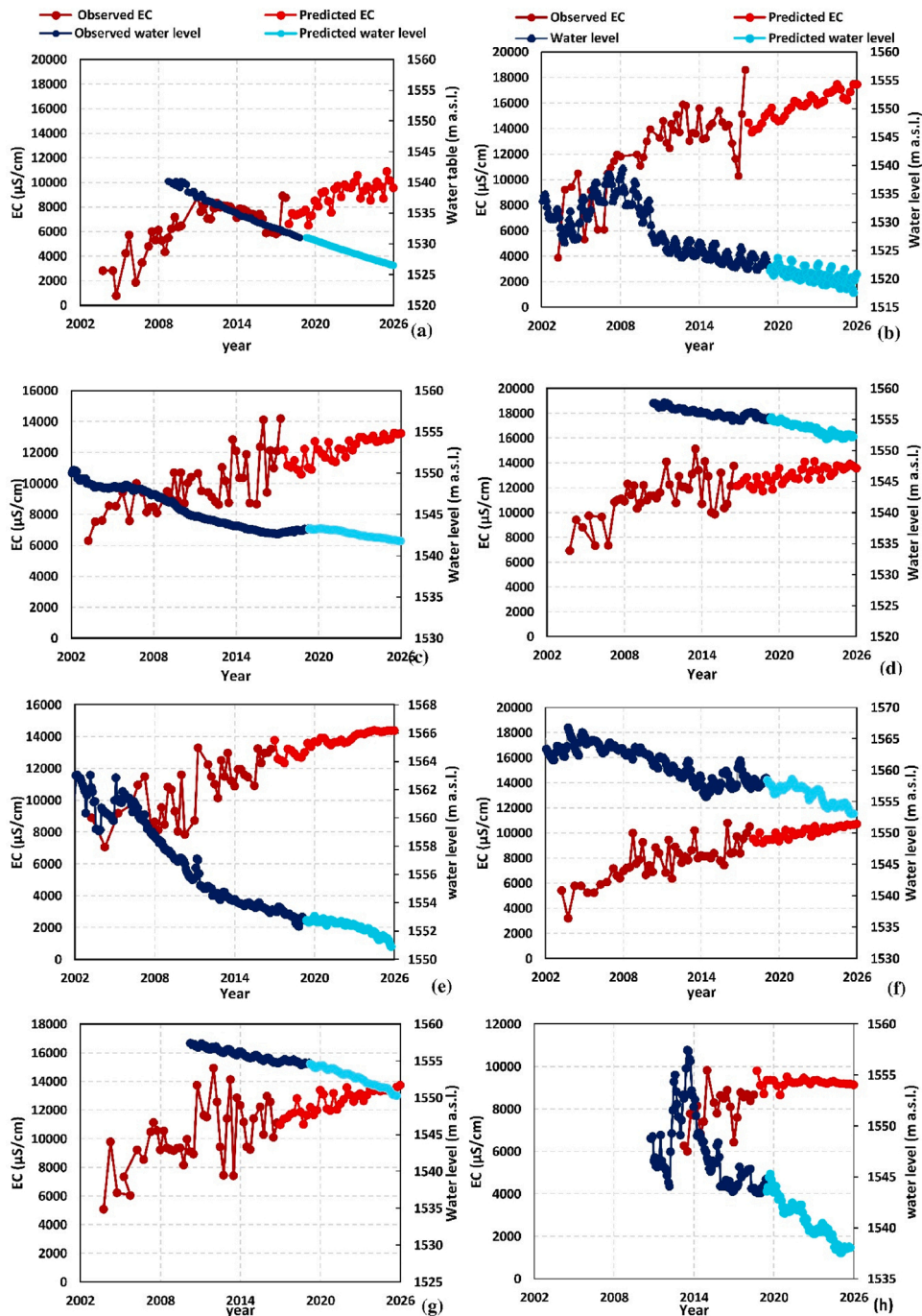
Fig. 10. Selected pumping wells (red) and water level of selected piezometers in the Brackish Zone of: (a) Abadeh Tashk aquifer, (b) Kharameh aquifer,(c) Neyriz aquifer, (d) Tang Hana aquifer, (e) Tavabe Arsangan aquifer, (f) Khir aquifer, (g) Pichkan aquifer, and (h) Kaneh kat aquifer.

differences in salinity between the three zones BZ, TZ, and FZ, also the chemical signature is different as well as characteristic of these zones. The Piper (262 typical wells in 2009) plots of major cations and anions in groundwater samples of the study area are shown in Fig. 8.a. The Piper diagram shows the presence of various hydrochemical facies that were observed in the groundwater samples, such as Ca-HCO$_3$, Na-HCO$_3$, Na-SO$_4$, Ca-SO$_4$, Mg-Cl, Ca-Cl and Na-Cl types. The dominant chemical facies in water are Ca-Cl and Na-Cl types. The water samples of the coastal aquifer are predominantly of the Cl– type (83%), and some of the HCO$_3$- type (13.6%) and SO$_4^{2-}$ type, (3.4%), respectively.

The FZ samples distributed in the left corner of the piper diagram are mainly represented by Ca and Mg bicarbonate (Ca-Mg-HCO$_3$) type water. This type of water naturally evolves by contact with predominantly limestone and dolomitic strata and cements in the

Table 4

Statistical criteria of the training data for SVR algorithms on BTL coastal aquifers.

Aquifer name	Abadeh	Pichkan	Tavabe Arsanjan	Tang Hana	Neyriz	Khir	Khrameh	Khanekat
EC								
R-squared	0.70	0.65	0.77	0.77	0.67	0.73	0.64	0.68
RMSE	1201.8	974.8	586.4	1037.8	1504.2	729.3	2794.7	2819
MAPE	12.6	6.8	3.1	6.1	9.1	5.1	15.7	17
MAE	1039.9	678.7	438.6	789.6	1194.7	524.5	2328.0	2400
Groundwater level								
R-squared	0.99	0.99	0.99	0.91	0.98	0.88	0.9	0.6
RMSE	0.06	0.003	0.007	0.18	1.60	1.0	3.8	1.68
MAPE	0.003	0.000	0.01	0.01	0.02	0.0	0.2	0.086
MAE	0.05	0.003	0.01	0.15	0.01	0.7	3.1	1.25

recharge area. The TZ water samples from places that are located between the two endmembers fresh water and lake are indicative of mixing, leading to a water composition with partially bicarbonates of Ca and Mg, and Na-Cl types.

The water type of the BZ samples that are close to BTL is of the Na-Cl type and due to intrusion of BTL water as far as the coast aquifers are concerned. The saline samples occupy the right top section and have been obtained near the boundary of BZ and TZ. Their chemical properties are controlled by alkaline earth cations and chloride. This process occurs under conditions of saltwater intrusion which leads to the change of water facies from Na-Cl to Ca-Cl type (Xue et al., 1995; Appelo and Postma, 2005; Han et al., 2014; Najib et al., 2017; Eeman et al., 2016; Abu-alnaeem et al., 2018; Nogueira et al., 2019; Telahigue et al., 2020). Regarded as an important water end-member, the BTL water and brine under the lake are also plotted in the figure, and their water type is of the Na–Cl type.

The Piper diagram illustrates the different species that can be found in the water samples of different signatures. This is confirmed in the Gibbs diagram (Fig. 8.b). This diagram shows the TDS concentration is a function of the ratio between Cl- and Cl- + HCO3-, showing a distinct gradual change from lake water quality towards the freshwater, that is dominated by chemical interaction between calcareous rock and groundwater. With increasing TDS, the water quality changes from freshwater to transition (due to mixing of freshwater with intruding lake water, towards the lake's water composition). However, it is evident that the so-called brackish water (BZ) is significantly less saline than the lake itself.

5.6. Conceptual model of the BTL coastal aquifers

The hydrogeological, geochemical and hydraulic data were combined to develop a conceptual model for SWI into the coastal aquifers of BTL (Fig. 9). The model consist of 5 zones BrZ, HSZ, BZ, TZ and FZ, using abbreviations introduced in section 5.4. The type of water is Na-Cl in the first three zones but it changes to mixed Ca-Na-Cl-HCO3 in TZ and Ca-HCO3 in the fresh zone. The right and the left sides of this figure are the land boundary and the lake, respectively. At the lake side, h_s denotes the level of the lake water, and at the land side, h_f is the freshwater table. Whereas often in SWI studies, h_s is constant, here it appears that h_s is not constant. TDS of pore water under the lake decreases from the center of lakes to the coast. Not only does the head of lake water or brine under the lake decrease as the distance to the lake center increases, but also this level continues to decrease as a function of time. The regional head difference between the center of the lake and the Transition Zone (TZ) is the force driving groundwater flow towards this TZ. An additional driving force, though, is the gradient in salinity and therefore in density of the pore water, which decreases in the same direction as the decreasing groundwater head. As the salinity is quite significant, so is the density difference (with average density at the lake side of 1.259 g/cm^3). Accordingly, we can speak for the coastal aquifers of active SWI (Werner et al., 2013), where the driving force due to density gradients enhance that due to the water level differences.

Since under more or less constant water density, the land side of the aquifers experience fresh groundwater flow, this fresh groundwater flow meets that coming from the lake at the Transition Zone. In part near of the coastal aquifer, due to excessive salinity it is already no longer possible to use the water pumped up by wells. Natural causes as well as human influence, especially groundwater pumping from coastal freshwater wells, have increased saltwater intrusion in many coastal areas (Ferguson and Gleeson, 2012; Lu et al., 2013a). In the present case, the conventional circulation of saline water at the interface of saline and freshwater, back to lake does not significantly occur. The main reason is that the interface is located at the area where wells are pumping up the water. The sources of water that replenishes the coastal aquifers are infiltrating rainwater, agricultural return flows, and inflow from the adjacent karstic formations. The source of salinity is the salt that originates from both the lake and underlying brine and salt marsh. The EC of exploitation wells is generally less than 20000 μS/cm, because the farmers usually reduce the well depth to prevent the deteriorating water quality due to upconing. This is also apparent from the well depths that generally increase away from the lake coast, because the depth to saline-brackish interface increases.

5.7. Temporal variation and forecasting of groundwater salinity and level

The time series of measured EC and groundwater level show, both for the recent past and the near future, a groundwater level decline and EC rise, for the period of 2002 to 2026 (Fig. 10).The statistical criteria of accuracy of training datasets are presented in Table 4. The water level in piezometers decreases in all the coastal aquifers in the Brackish zone, but the EC does not follow the gradual

decreasing trend of water table, and its variation is high in all coastal aquifers. In spite of the dropping water table, the EC is almost constant or even a slight decreasing trend in some of the coastal aquifers. The number of piezometers is limited and their distance with pumping wells is regulated to be out of the depression cone of the pumping wells, therefore the decreasing trend of water level in piezometers is due to total overexploitation of coastal aquifers. The depth of water inside the wells is shallow and EC of water below the well bottom is high in the pumping wells of the Brackish zone. As the discharge increases in a well, the water level inside that well decreases, consequently the EC increases. The salinity in a well is sensitive to discharge duration of exploited water use of that pumping well, and water demand (type of crops). The EC of each pumping well also depends on farmer management. As the salinity increases in a pumping well, the farmer reduces the EC by the management strategy such as reducing the discharge, and water demand by changing the type of crop. Therefore, the constant EC or even a narrow decreasing trend is a management strategy and it does not affect the water level in the piezometer. Discharges that increase have a significant effect on the dropping water table in pumping well but no effect in piezometers far from pumping well.

The crops with high tolerance to salinity are cultivated in spite of drastically production reduction. There is no official systematic management program to reduce the overexploitation therefore, the water level decline and EC enhancement will be expected in the future (Fig. 10).

The main constraint is the water table must be controlled at a specific level, because a) the wells may fall dry due to shallow wells depth, b) the farmers based on their experience reduce the discharge to prevent a further drop in well level in spite of these constraints, the active intrusion advances into the brackish zone due to the hydraulic gradient force.

The predicted results of EC and water level in the Bakhtegan-Tashk catchment area highlighted an environmental crisis of the groundwater and lake of being seriously subject to declining water level and high rates of saline water intrusion.

It is highly recommended that must stop exploitation of groundwater in the Brackish zone to prevent increasing saltwater intrusion and soil salinity. Management of water resources exploitation is necessary to ensure a balance between recharge and pumping from groundwater. Future plans i.e., numerical modeling must be developed to use sustainable consumption of groundwater to avoid groundwater salinization. However, as America et al. (2020) showed, such modelling may have an even higher demand of data input in view of the complexities of the fresh/salt groundwater system (Table 4).

6. Conclusions

The original and natural general flow direction was directed from the coastal aquifers towards the BTL. However, we have established that currently, the general flow direction has reversed from the BTL or salt marsh towards the adjacent aquifers. This is demonstrated by the iso-potential lines of 2004, 2009, 2017, and several other years in both wet and dry months. The main reason of this reversal is the over-exploitation of the adjacent aquifers that cause the decline of the water tables to below the BTL water level, even though the water levels of BTL itself are also dropping. In addition, the average salinity of the BTL has also increased profoundly from a TDS of 45400 mg/l before 2007 to about 256000 mg/l after shrinkage. This has increased the salinity and therefore water density gradient, which implies stronger buoyancy forces that also induce flow from the BTL toward the adjacent aquifers.

In this study, we developed an active saltwater intrusion (SWI) conceptual model for the BTL and the coastal aquifers under overexploitation. Spatial analysis of active SWI showed that for most of the coastal aquifers five zones can be distinguished, with different hydro-chemical signatures, namely: the Brine Zone (BrZ), Highly Saline Zone (HSZ), Brackish Zone (BZ), Transition Zone (TZ) and Fresh Zone (FZ). BrZ and HSZ are found in the area where production wells are lacking in view of the high salinity, with an EC of more than 20000 μS/cm. BZ is an area that is severely affected by active SWI and the chemical water is type is 100% Cl-. TZ with narrow width, has special characteristics, namely a) it shows mixing of fresh and brackish zones, b) it has the lowest water levels in the study area, c) it comprises the farthest inland toe of salt/fresh-interface movement of active SWI, and d) has a significant salinity gradient at the boundary between the BZ and TZ. FZ is entirely recharged by the Karstic formation and the water type is 100% HCO_3-. Hydro-chemical variation Piper and Gibbs diagrams confirm our classification of coastal aquifer zones. Based on the conceptual model developed presently, the conventional circulation of saline water at the interface of saline and freshwater, back to lake is almost absent.

The SVR modelling revealed how the salinity grows, while the water level further drops continuously from 2002 to 2026 in the coastal aquifers. This robust forecasting of future EC values and water level for short to intermediate periods (about equal to the experimental data period) is useful approach for developing sustainable and groundwater resource management strategies for the future, and may help to prioritize remedial actions for the different aquifers. As we have established, lake brine gradually intrudes further into the fresh coastal aquifers. This is a threat, as clearly the aquifer suffers from over-exploitation which disagrees with sustainable water management in the region. It is apparent that the current situation of active SWI is indicative of the need to develop a regional freshwater management plan.

CRediT authorship contribution statement

Maryam Vahidipour: Investigation, Methodology, Formal analysis, Writing - original draft. **Ezzat Raeisi:** Supervision, Project administration, Conceptualization, Formal analysis, Resources, Funding acquisition, Writing - review & editing. **Sjoerd E.A.T.M. van der Zee:** Supervision, Methodology, Resources, Funding acquisition, Writing - review & editing.

Declaration of Competing Interest

The authors report no declarations of interest.

Acknowledgement

Appendix A. Supplementary data

Supplementary material related to this article can be found, in the online version, at doi:https://doi.org/10.1016/j.ejrh.2021.100790.

References

Abu-alnaeem, M.F., Yusoff, I., Ng, T.F., Alias, Y., Raksmey, M., 2018. Assessment of groundwater salinity and quality in Gaza coastal aquifer, Gaza Strip, Palestine: An integrated statistical, geostatistical and hydrogeochemical approaches study. Science of the Total Environment. 615, 972–9989. https://doi.org/10.1016/j.scitotenv.2017.09.3200.

Agard, P., Omrani, J., Jolivet, L., Mouthereau, F., 2005. Convergence history across Zagros (Iran): constraints from collisional and earlier deformation. International Journal of Earth Sciences. 94 (3), 401–419. https://doi.org/10.1007/s00531-005-0481-4.

Afrasiabi, B., Sedghi Asl, M., 2015. Estimation of geostatistics methods for groundwater qualitative estimation of Niriz plain of Fars provinc. 10th International Congress on Civil Engineering, Faculty of Civil Engineering, Tabriz. https://www.civilica.com/Paper-ICCE10-ICCE10_1090.html.

Agh, N., 2007. Characterization of Artemia populations from Iran. Aristotle University of Thessaloniki, Greece.

Ahmadianfar, I., Jamei, M., Chu, X., 2020. A novel Hybrid Wavelet-Locally Weighted Linear Regression (W-LWLR) Model for Electrical Conductivity (EC) Prediction in Surface Water. Journal of contaminant hydrology 232, 103641. https://doi.org/10.1016/j.jconhyd.2020.103641.

Alavi, M., Mahdavi, M., 1994. Stratigraphy and structures of the Nahavand region in western Iran, and their implications for the Zagros tectonics. Geological Magazine. 131 (1), 43–47. https://doi.org/10.1017/S0016756800010475.

America, I., Zhang, C., Werner, A.D., van der Zee Sjoerd, E.A.T.M., 2020. Evaporation and salt accumulation effects on riparian freshwater lenses. Water Resources Research 56. https://doi.org/10.1029/2019WR026380 e2019WR026380.

Appelo, C.A.J., Postma, D., 2005. Geochemistry, groundwater and pollution, 2nd edition. A.A. Balkema, Leiden, The Netherlands, p. 649.

Argamasilla, M., Barberá, J.A., Andreo, B., 2017. Factors controlling groundwater salinization and hydrogeochemical processes in coastal aquifers from southern Spain. Science of the Total Environment. 580, 50–68. https://doi.org/10.1016/j.scitotenv.2016.11.173.

Badaruddin, S., Werner, A.D., Morgan, L.K., 2015. Watertable salinization due to seawater intrusion. Water Resour. Res. 51, 8397–8408. https://doi.org/10.1002/2015WR01709.

Badaruddin, S., Werner, A.D., Morgan, L.K., 2017. Characteristics of active seawater intrusion. Journal of Hydrology. 551, 632–647. https://doi.org/10.1016/j.jhydrol.2017.04.031.

Bastani, M., Rakhshandehroo, G.R., 2010. Inverse modeling of variable-density groundwater flow in a semi-arid area in Iran using a genetic algorithm. Hydrogeology journal 18 (5), 1191–1203. https://doi.org/10.1007/s10040-010-0599-8.

Bear, J., 1979. Hydraulics of Groundwater. McGraw-Hill, New York, p. 569.

Bear, J., 1972. Dynamics of Fluids in Porous Media. Soil Sci. 120, 162–163. https://doi.org/10.1097/00010694-197508000-00022.

Berberian, M., 1995. Master blind thrust faults hidden under the Zagros folds: Active basement tectonics and surface morphotectonics. Tectonophysics. 241, 193–224. https://doi.org/10.1016/0040-1951(94)00185-C.

Bureau of Reclamation, 2003. Desalting handbook for planners, 3d ed. Bureau of Reclamation, Washington D.C. 310 p.

Delsman, J.R., Huang, K.R.M., Vos, P.C., de Louw, P.G.B., Oude Essink, G.H.P., Stuyfzand, P.J., Bierkens, M.F.P., 2014. Paleo-modeling of coastal saltwater intrusion during the Holocene: an application to the Netherlands. Hydrol. Earth Sys. Sci. 18, 3891–3905. https://doi.org/10.5194/hess-18-3891-2014.

Eeman, S., De Louw, P.G.B., Van der Zee, S.E.A.T.M., 2016. Cation exchange in a temporally fluctuating thin freshwater lenson top of saline groundwater. Hydrogeol J. https://doi.org/10.1007/s10040-016-1475-y.

Fars Regional Water Authority (FRWA), 2009. Updating Atlas studies of water resources Tashak - Bakhtegan and Maharloo lakes catchment area, Fars, Iran.

Fars Regional Water Authority (FRWA), 2016. Updating studies of water budget of water resources in Tashak - Bakhtegan and Maharloo lakes catchment area, Fars, Iran.

Fars Regional Water Authority (FRWA), 2018. Unit hydrographs of Bakhtegan Tashk catchment area, Fars, Iran.

Fetter, C.W., 2001. Appl. Hydrogeol. Prentice Hall Inc., New Jersey, p. 598.

Ferguson, G., Gleeson, T., 2012. Vulnerability of coastal aquifers to groundwater use and climate change. Nat. Clim. Change. 2, 342–345. https://doi.org/10.1038/nclimate1413.

Fotooli, B., 2002. Bakhtegan management integrated plan studies. Environmental Protection Agency, 157p (In Persian).

Freeze, R.A., Cherry, J.A., 1979. Groundwater. Englewood Cliffs, N.J., Prentice Hall, 604.

Ganjali, S., Ildoromi, A., 2012. Investigation of changes in landand water boundary in conservation areas of Anzali wetland by using GIS. J Wetl Ecobiol. 3, 59–68.

Geological Survey of Iran, 2002. Report of Arsanjan Sheet (scale: 1/100000).

Gibbs, R.J., 1970. Mechanisms controlling world water chemistry. Science. 170, 795–840.

Han, D.M., Song, X.F., Currell, M.J., Yang, J.L., Xiao, G.Q., 2014. Chemical and isotopic constraints on evolution of groundwater salinization in the coastal plain aquifer of Laizhou Bay, China. Journal of Hydrology 508, 12–27. https://doi.org/10.1016/j.jhydrol.2013.10.040.

Hem, J.D., 1985. Study and interpretation of the chemical characteris-tics of natural water. U.S. Geol. Surv. Water Suppl. Pap. 2254, 1–263.

Hubert, E., Wolkersdorfer, C., 2015. Establishing a conversion factor between electrical conductivity and total dissolved solids in South African mine waters. Water SA41, 490–500.

Ju, Y., Massoudieh, A., Green, C.T., Lee, K.K., Kaown, D., 2020. Complexity of groundwater age mixing near a seawater intrusion zone based on multiple tracers and Bayesian inference. Science of The Total Environment 753, 141994. https://doi.org/10.1016/j.scitotenv.2020.141994.

Kazakis, N., Pavlou, A., Vargemezis, G., Voudouris, K.S., Soulios, G., Pliakas, F., Tsokas, G., 2016. Seawater intrusion mapping using electrical resistivity tomography and hydrochemical data. An application in the coastal area of eastern Thermaikos Gulf, Greece. Science of the Total Environment. 543, 373–387. https://doi.org/10.1016/j.scitotenv.2015.11.041.

Khadra, W.M., Stuyfzand, P.J., van Breukelen, B.M., 2017. Hydrochemical effects of saltwater intrusion in a limestone and dolomitic limestone aquifer in Lebanon. Applied Geochemistry 79, 36–51. https://doi.org/10.1016/j.apgeochem.2017.02.005.

Langevin, C., Shoemaker, W.B., Guo, W., 2003. Modflow, 2000, The USGS Geological Survey modular ground-water model – documentation of the Seawat-2000 version with the variable density flow process (VDF) and the integrated MT3DMS transport process (IMT). US Geological Survey Open-File Report, pp. 03–426.

Loffler, H., 1961. Contributions to knowledge of the Iranian Inland Water I1: Regional limnological study with special consideration the crustacean fauna. Int. Revueges.Hydrobio1 46, 309–406.

Lu, C., Werner, A.D., Simmons, C.T., 2013a. Threats to coastal aquifers. Correspondence. Nat. Clim. Change. 3, 605. https://doi.org/10.1038/nclimate1901.

Mahlknecht, J., Merchán, D., Rosner, M., Meixner, A., Ledesma-Ruiz, R., 2017. Assessing seawater intrusion in an arid coastal aquifer under high anthropogenic influence using major constituents, Sr and B isotopes in groundwater. Science of the Total Environment 587–588, 282–295. https://doi.org/10.1016/j.scitotenv.2017.02.137.

Meyer, J.E., Wise, M.R., Kalaswad, S., 2011. Pecos Valley aquifer, west Texas—Structure and brackish groundwater. Texas Water Development Board Report, Austin, TX, 85 p.

Mohammadi, E., 2020. Hydrology and wind erosion potential of Tashk and Bakhtegan lakes. Masters thesis. Shiraz university, Shiraz, Iran.

Morgan, L.K., Werner, A.D., 2015. A national inventory of seawater intrusion vulnerability for Australia. J. Hydrol. Regional Studies. 4, 686–698. https://doi.org/10.1016/j.ejrh.2015.10.005.

Najib, S., Fadili, A., Mehdi, K., Riss, J., Makan, A., 2017. Contribution of hydrochemical and geoelectrical approaches to investigate salinization process and seawater intrusion in the coastal aquifers of Chaouia, Morocco. Journal of contaminant hydrology 198, 24–36. https://doi.org/10.1016/j.jconhyd.2017.01.003.

National Ground Water Association, 2010. Brackish groundwater.Westerville, Ohio. National Ground Water Association information brief, 4 p.

Nejati, M., 1994. Investigation of saline water intrusion in karstic spring south of Abade Tashk. Master thesis. Shiraz University, Shiraz, Iran.

Nogueira, G., Stigter, T.Y., Zhou, Y., Mussa, F., Juizo, D., 2019. Understanding groundwater salinization mechanisms to secure freshwater resources in the water-scarce city of Maputo, Mozambique. Science of The Total Environment 661, 723–736. https://doi.org/10.1016/j.scitotenv.2018.12.343.

Phan, T.T.H., Nguyen, X.H., 2020. Combining Statistical Machine Learning Models with ARIMA for Water Level Forecasting: The Case of the Red River. Advances in Water Resources. https://doi.org/10.1016/j.advwatres.2020.103656.

Piper, A.M., 1944. Graphic procedure in the geochemical interpretation of water analyses. Trans Am Geophys. 25, 914–928.

Rainwater, F.H., Thatcher, L.L., 1960. Methods for collection and analysis of water samples. Report No 1454 (U. S. Govt. Print. Off., 1960).

Ramsar Convention, 2016. The List of Wetlands of International Importance (the Ramsar List). Retrieved from. http://www.ramsar.org/.

Reese, R.S., 1994. Hydrogeology and the distribution and origin of salinity in the Floridan aquifer system, southeastern Florida. U.S. Geological Survey Water-Resources Investigations Report, 94–4010, 56 p.

Rezaei, M., 1998. Hydrogeology of karst chloride springs in the Rahmat anticline. Master thesis. Shiraz University, Shiraz, Iran.

Rhoades, J.D., Kandiah, A., Mashali, A., 1992. The use of Saline Waters for Crop Production. FAO.

Robinove, C.J., Langford, R.H., Brookhart, J.W., 1958. Saline water resources of North Dakota. U.S. Geological Survey Water-Supply Paper 1428, 72 p.

Shiri, J., Kisi, O., Yoon, H., Lee, K.K., Nazemi, A.H., 2013. Predicting groundwater level fluctuations with meteorological effect implications—A comparative study among soft computing techniques. Computers & Geosciences 56, 32–44. https://doi.org/10.1016/j.cageo.2013.01.007.

Small, C., Nicholls, R.J., 2003. A global analysis of human settlement in coastal zones. J Coast Res. 19 (3), 584–599. http://www.jstor.org/stable/4299200.

Stanton, J.S., Anning, D.W., Brown, C.J., Moore, R.B., McGuire, V.L., Qi, S.L., Harris, A.C., Dennehy, K.F., McMahon, P.B., Degnan, J.R., Böhlke, J.K., 2017. Brackish groundwater in the United States. U.S. Geological Survey Professional Paper. 1833. https://doi.org/10.3133/pp1833, 185 p.

Stocklin, J., Setudehnia, A., 1977. Stratigraphic lexicon of Iran. Geological Survey of Iran, Tehran.

Stoeckl, L., Walther, M., Morgan, L.K., 2019. Physical and Numerical Modelling of Post-Pumping Seawater Intrusion. Geofluids 2019. https://doi.org/10.1155/2019/7191370.

Telahigue, F., Mejri, H., Mansouri, B., Souid, F., Agoubi, B., Chahlaoui, A., Kharroubi, A., 2020. Assessing seawater intrusion in arid and semi-arid Mediterranean coastal aquifers using geochemical approaches. Physics and Chemistry of the Earth, Parts A/B/C 115, 102811. https://doi.org/10.1016/j.pce.2019.102811.

Thorslund, J., van Vliet, M.T., 2020. a global dataset of surface water and groundwater salinity measurements from 1980–2019. Scientific Data 7 (1), 1–11. https://doi.org/10.1038/s41597-020-0562-z.

Torabi Haghighi, A., Kløve, B., 2017. Design of environmental flow regimes to maintain lakes and wetlandsin regions with high seasonal irrigation demand. Ecological Engineering 100, 120–129.

Van der Zee, S.E.A.T.M., Shah, S.H.H., Vervoort, R.W., 2014. Root zone salinity and sodicity under seasonal rainfall due to feedback of decreasing hydraulic conductivity. Water Resour. Res. 50, 9432–9446. https://doi.org/10.1002/2013WR015208.

Vapnik, V.N., 1995. The Nature of Statistical Learning Theory. Springer-Verlag, Berlin, Heidelberg.

Vázquez-Suñé, E., Abarca, E., Carrera, J., Capino, B., Gámez, D., Pool, M., Simó, T., Batlle, F., Niñerola, J.M., Ibañez, X., 2006. Groundwater modelling as a tool for the European Water Framework Directive (WFD) application: the Llobregat case. Phys. Chem. Earth 31, 1015–1029. https://doi.org/10.1016/j.pce.2006.07.008.

Walther, M., Leonard, S., 2020. Post-pumping seawater intrusion at the field scale: Implications for coastal aquifer management. Advances in Water Resources, p.103561. https://doi.org/10.1016/j.advwatres.2020.103561.

Werner, A.D., 2017. On the classification of seawater intrusion. Journal of Hydrology 551, 619–631. https://doi.org/10.1016/j.jhydrol.2016.12.012.

Werner, A.D., Bakker, M., Post, V.E.A., Vandenbohede, A., Lu, C.H., Ataie-Ashtiani, B., Simmons, C.T., Barry, D.A., 2013. Seawater intrusion processes, investigation and management: recent advances and future challenges. Adv. Water Resour. 51, 3–26. https://doi.org/10.1016/j.advwatres.2012.03.004.

Werner, A.D., Gallagher, M.R., 2006. Characterisation of sea-water intrusion in the Pioneer Valley, Australia using hydrochemistry and three-dimensional numerical modelling. Hydrogeol. J. 14, 1452–1469. https://doi.org/10.1007/s10040-006-0059-7.

Winslow, A.G., Hillier, D.E., Turcan, A.N.J., 1968. Saline ground water in Louisiana. U.S. Geological Survey Hydrologic Atlas 310, 4 pls. 1:750,000.

Xue, Y.Q., Xie, C.H., Wu, J.C., Liu, P.M., Wang, J.J., Jiang, Q.B., 1995. A three dimensional miscible transport model for seawater intrusion in China. Water Resour. Res. 31, 903–912. https://doi.org/10.1029/94WR02379.

Yakirevich, A., Melloul, A., Sorek, S., Shaath, S., Borisov, V., 1998. Simulation of seawater intrusion into the Khan Yunis area of the Gaza Strip coastal aquifer. Hydrogeol. J. 6, 549–559. https://doi.org/10.1007/s100400050175.

Yobbi, D.K., 1996. Simulation of the subsurface storage and recovery of treated effluent injected in a saline aquifer. St. Petersburg, Florida: U.S. Geological Survey Water-Resources Investigations Report 95–4271, 29 p.